D. Elwood
S.C. Yim

School of Civil and Construction Engineering
Oregon State University

E. Amon
A. von Jouanne
T.K.A Brekken

School of Electrical Engineering and Computer Science

Estimating the Energy Production Capacity of a Taut-Moored Dual-Body Wave Energy Conversion System Using Numerical Modeling and Physical Testing

This paper presents an innovative technique for evaluating the performance of direct-drive power take-off systems for wave energy devices using simulated force and velocity profiles. The performance of a linear generator was evaluated in a realistic operating condition using the results from a coupled model of a taut moored, dual body, wave energy conversion system as position input for Oregon State's wave energy Linear Test Bed. The experimental results from the Linear Test Bed can be compared with the predictions of the simulation and used to evaluate the efficiency of the generator.

1 INTRODUCTION

Modern ocean wave-energy research began during the oil crisis of the 1970s. Much of the early work was conducted in Europe by Salter (Salter 1976) and Evans (Evans 1979) in England and Falnes (Falnes 2002) and Budal (Budal 1977) in Norway, amongst others. Several promising concepts were developed by 1980 including point absorber wave energy converters such as the infamous Salter duck (Salter 1976) and oscillating water column (OWC) devices. Point absorbers extract energy from ocean waves by capturing the mechanical energy from the dynamic response of one or more floating bodies. If energy is extracted from a single degree of freedom (DOF) these devices can extract at most 50% of the wave energy (Evans 1979). Oscillating water column systems gather energy from the waves by converting pneumatic pressure generated by waves rising and falling in a sealed chamber into electricity. Electricity is generated by using the changing wave level to generate air flow through a nozzle driving a Wells turbine (Curran R. 1997). Early work was also conducted on the optimal control of wave energy devices (Budal 1977) (Falnes 2002). By controlling the power take-off the natural frequency of the system could be varied keeping the system in resonance with the wave forcing.

Currently, several commercial developers are working to build full scale, grid connected wave energy conversion systems. These include the Limpet (WaveGen 2008) oscillating water column, the Pelamis (Pelamis Wave Power 2008) attenuating wave-energy conversion system , and the Archimedes Wave Swing (Archimedes Wave Swing 2008). In the United States, Ocean Power Technologies (Ocean Power Technologies 2008) developed a point absorber wave energy conversion buoy for the US Navy that has been tested off Oahu, Hawaii. OPT has plans to deploy an array of point absorber buoys off the coast of Reedsport, Oregon representing the first grid connected wave energy conversion plant in the United States.

The SeaBeavI, a 1kW direct-drive wave energy conversion system, was designed and built by researchers at Oregon State starting in the fall of 2006. The SeaBeavI is a taut moored, dual body point absorber utilizing a linear generator for power take-off (Prudell 2007). The central spar is taut moored to the bottom and holds the armature of the linear generator. The outer taurus shaped buoy is free to heave relative to the spar creating electricity as the magnet section moves relative to the copper wires in the armature. In October of 2007 the device was tested in the open ocean off Newport, Oregon. A rendering of the SeaBeavI is included as Figure 1.

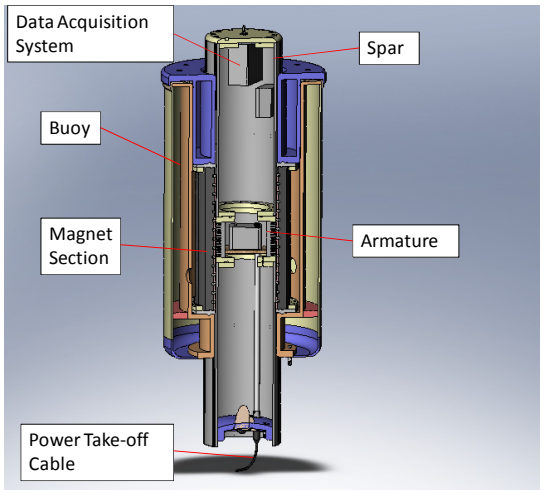

Figure 1 Rendering of spar and buoy general arrangement

2 SYSTEM CONFIGURATION

After testing of the SeaBeavI it was determined that the waterplane stiffness of the buoy was insufficient to provide the force required to drive the linear generator. Additionally, the excess buoyancy of the spar was not great enough to keep the mooring in tension during the down stroke of the buoy. The diameter of the buoy was increased, adding hydrostatic stiffness, and a circular footing was added to the spar in order to increase the pre-tension in the mooring. The geometry of the resized SeaBeavI is shown in Figure 2. As shown in the figure, the overall depth of the redesigned system was increased to 7.5 m with a maximum buoy diameter of 2 m. The displacement of the spar was increased to 6350 kg with a total spar mass of 1454 kg. This led to a design mooring pre-tension of 48029 N. The mooring system connecting the spar to the ocean floor is a single tensioned leg composed of chain, spectra rope, and a mid-column float.

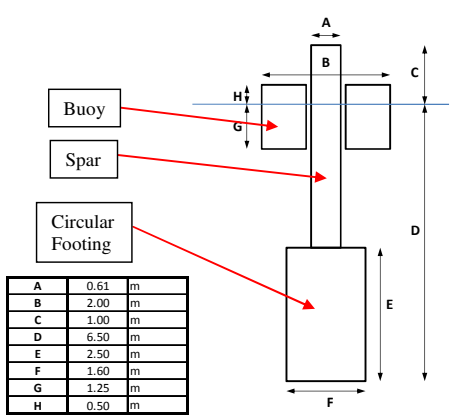

A	0.61	m
B	2.00	m
C	1.00	m
D	6.50	m
E	2.50	m
F	1.60	m
G	1.25	m
H	0.50	m

Figure 2 Geometry of the resized SeaBeavI

3 ORCAFLEX MODEL

OrcaFlex is a coupled analysis numerical code designed to model the dynamics of offshore structures. The code has a range of capabilities from the modeling of mooring and riser systems to analysis of towed bodies and marine renewable energy systems. The coupled modeling technique used by OrcaFlex combines a finite element model of the flexible mooring and riser components with a rigid body representation of a floating system (Orcina Ltd. 2007). Hydrodynamic forces on the floating system and lines are calculated using a Morison model approach. Multiple floating bodies can be linked together using both linear and non-linear springs and dampers.

To calculate the response of the dynamic system, OrcaFlex solves the following equation of motion in the time domain (Orcina Ltd.):

$$M(d,a) + C(d,v) + K(d) = F(d,v,t) \qquad (1)$$

where

M(p,a) is the inertial load
C(p,v) is the damping load
K(p) is the system stiffness
F(p,v,t) is the external load
d, v, a are the displacement, velocity, and acceleration vectors
t is the simulation time

4 HYDRODYNAMIC MODEL

In order to calculate the hydrodynamic forces on the buoy and spar, OrcaFlex uses a modified form of the Morison equation originally developed to calculate wave forces on fixed cylinders. The primary difference between the classical Morison equation and the modified form used for floating bodies is that the relative velocity between the body and the fluid is used to calculate the damping force and the relative acceleration is used to calculate the added mass. The modified Morison equation used by OrcaFlex lead to the following expression for the wave forcing:

$$F_w = (\Delta a_w + C_a \Delta a_r) + {}^1\!/_2\, \rho V_r |V_r| C_D A \qquad (2)$$

where

F_w is the wave force
Δ is the mass of water displaced by the body
C_a is the added mass coefficient
V_r is the fluid velocity relative to the body
a_r is the fluid acceleration relative to the body
ρ is the density of water
C_D is the drag coefficient

A is the drag area

For analysis of the wave-energy conversion system, both the spar and buoy were modeled as spar buoys in OrcaFlex. This type of buoy is composed of a vertical stack of cylinders each with its own added mass, damping, and drag properties. The inertial forces on each cylinder are calculated using user supplied axial and normal added mass coefficients. Likewise, the components of the force due to the fluid velocity are calculated using user supplied axial and normal unit damping forces. The instantaneous wetted surface of each cylinder is calculated for each time step and a correction factor is applied to the added mass and damping. This leads to the following expression for the added mass:

$$F_{x-AddedMass} = PW(\Delta_c A_x + C_{an}\Delta_c A_{rx}) \quad (3)$$
$$F_{y-AddedMass} = PW(\Delta_{cy} A_y + C_{an}\Delta_c A_{ry}) \quad (4)$$
$$F_{z-AddedMass} = PW(\Delta_c A_z + C_{aa}\Delta_c A_{rz}) \quad (5)$$

where

PW is the proportion wet for the cylinder
Δ_c is the displaced mass of the cylinder when it is fully submerged
A_x, A_y, A_z are the components of the fluid acceleration (buoy coordinates)
A_{rx}, A_{ry}, A_{rz} are the components of the fluid acceleration relative to the buoy
C_{aa}, C_{an} are the axial and normal added mass coefficients

Similarly the hydrodynamic damping on each cylinder is calculated using user supplied normal and axial unit damping forces:

$$F_{x-Damping} = PW * UDF_n * V_{rx} \quad (6)$$
$$F_{y-Damping} = PW * UDF_n * V_{ry} \quad (7)$$
$$F_{z-Damping} = PW * UDF_a * V_{rz} \quad (8)$$

where

V_{rx}, V_{ry}, V_{rz} are the components of the fluid velocity relative to the buoy
UDF_n, UDF_a are the user supplied normal and axial unit damping forces

The added mass and damping coefficients for the spar were based on experimental results (Chung 1993). Chung conducted a series of experiments to measure the heave added mass and damping of a surface piercing cylindrical buoy with a cylindrical base over a range of draft to diameter ratios. These empirical added mass and damping coefficients, input into OrcaFlex, can be found in the Appendix.

The added mass and damping coefficients for the buoy were based on the numerical results for a heaving circular cylinder in finite water depth (Bhatta 2007).The top of the circular footing of the spar was assumed to act like a false bottom and the distance between the bottom of the buoy and the top of the circular footing was taken as the water depth. This method assumes that the radiation and diffraction of the taurus shaped buoy heaving above a circular footing is equivalent to a buoy heaving with a water depth equal to the spacing between the footing and the bottom of the buoy. The added mass of the buoy in surge was determined using the analytical results for a circular cylinder (Newman 1977), and assumed to be a constant over the frequency range investigated. The added mass and damping coefficients used in the OrcaFlex model can be found in the Appendix.

5 MOORING MODEL

Lines are modeled in OrcaFlex using a finite element model. Each line is divided into a series of massless segments with a node at each end. These segments model the axial and torsional stiffness of the line while the mass, weight, and buoyancy of the line is incorporated into the end nodes. The bending stiffness of the line is represented by rotational springs linking the end nodes to the segment. Figure 3 shows the details of the line model with the three types of springs used to model the axial, torsional, and bending stiffness.

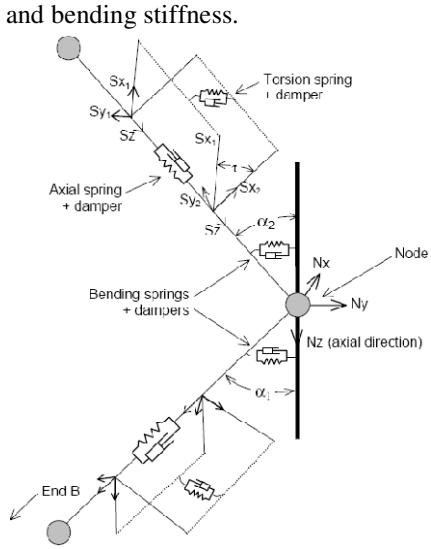

Figure 3 Graphical representation of OrcaFlex line model (Orcina 2006)

The mooring model created for the analysis of the resized SeaBeavI includes two lines and a subsurface float. The first line, connecting the subsurface float to the bottom, is 24 m long and is composed of 24 segments of uniform length. It is divided into two

sections with the bottom 13 m of the line having the properties of 5/8" chain and the top 11 m modeling 5/8" spectra rope. The subsurface float is modeled as a 1 m diameter sphere allowed to translate, but fixed in rotation. A second line connects the subsurface float to the spar and is 9.5 m long. This line has the properties of 5/8" spectra rope and is composed of 38 uniformly spaced segments.

6 WAVE MODEL

In order to understand the performance characteristics of the resized SeaBeavI wave energy conversion system, the response of the system was calculated in both regular and random waves. A model utilizing a Stokes 5th order wave theory was used to calculate the sea surface elevation along with the water particle velocities and accelerations for the simulations in regular waves. The spectrum used to generate the irregular waves was a modified Pierson-Moskowitz (ISSC) spectrum. The ISSC spectrum is defined in terms of the peak frequency (f_m) and the significant wave height (H_s):

$$S(f) = {}^{5}/_{16} H_s{}^2 f_m{}^4 f^{-5} e^{\left(-{}^{5}/_{4}\left({}^{f}/_{f_m}\right)^{-4}\right)} \tag{9}$$

where f is frequency

7 GENERATOR AND FRICTION MODELS

The generator and frictional forces due to the linear generator were incorporated into the OrcaFlex model using four linear springs, a linear damper, and a non-linear damper. The force due to the load on the generator was represented using a linear damper. The damping coefficients used were based on force characterization experiments run on the linear test bed (Elwood 2008). The contact friction between the spar and the buoy was represented by four linear springs and a non-linear damper. The linear springs provided the normal force while the non-linear damper represented the sliding friction. The friction characteristic was developed based on the LTB force characterization experiments.

Table 1: Stochastic Sea States Modeled in OrcaFlex

Hs(m)	Tp(s)	SS
0.1	7.5	1
0.3	7.5	2
0.5	7.5	2
0.88	7.5	3
1.25	7.5	3
1.88	8.8	4
2.5	8.8	4
3.25	9.7	5
4	9.7	5
4	9.7	5*
5	12.4	6*

*Survival Condition

8 LOAD CASES

The load cases investigated were selected to represent the range of design operating conditions for the device. The resized SeaBeavI was designed to operate in conditions up to sea state 5 and survive in up to a sea state 6. As such, the range of stochastic sea states investigated ranged from a 0.1m significant wave height with a 7.5 second peak period (SS1) to a 5m significant wave height with a 12.4 second peak period (SS6). Table 1 provides a list of the stochastic sea states simulated.

9 NUMERICAL RESULTS

The power captured by the device in stochastic seas increases proportional to the square of the significant wave height up to a wave height of 1.25m. Beyond 1.25m, the power increases linearly up to the operating limit of the device and then drops off considerably. In the survival condition, the mooring is slack allowing the spar and buoy to ride over the large waves. This reduces the relative motion between the two bodies and the power captured by the system. Figure 4 provides a plot of the power as a function of the significant wave height.

A standard measure used to evaluate the efficiency of wave energy conversion systems is the capture width. The capture width is defined as the ratio of the power captured by the device to the wave power per unit crest length:

$$C = \frac{P_c}{\frac{1}{8}\rho g H_{RMS}{}^2 C_g} \tag{10}$$

$$C_g = \frac{g T_P}{4\pi} \tag{11}$$

$$H_{RMS} = \frac{H_{1/3}}{\sqrt{2}} \tag{12}$$

where:

P_c is the mechanical powercaptured by the device
g is the gravitational acceleration
H_{RMS} is the RMS wave height
C_g is the deep water group velocity
T_P is the peak period
$H_{1/3}$ is the significant wave height

For the resized SeaBeavI, the capture width as a function of significant wave height is maximized for a significant wave height of 1.25m. Figure 5 provides a plot of the relationship between the significant wave height and the capture width.

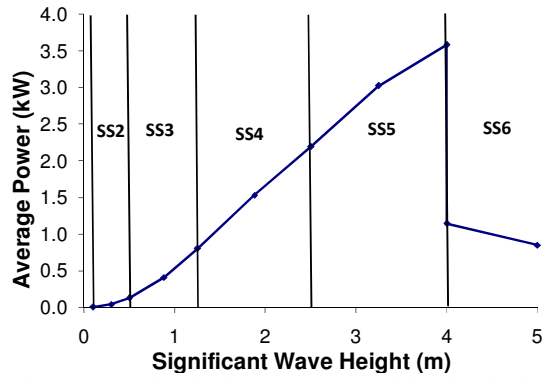

Figure 4 Mechanical power captured by the device as a function of the significant wave height

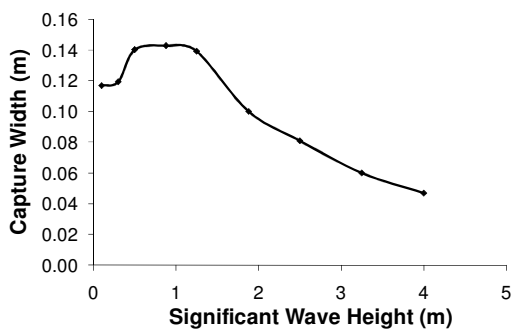

Figure 5 Relationship between the significant wave height and the capture width for the resized SeaBeavI wave energy conversion device

10 PHYSICAL EXPERIMENTS

The wave energy Linear Test Bed (LTB) at the Wallace Energy Systems & Renewables Facility, shown in Figure 6, was used to determine the efficiency of the permanent magnet linear generator in a realistic operating condition..

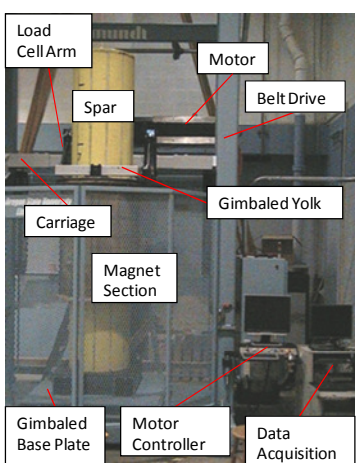

Figure 6 The active components of the permanent magnet linear generator mounted in OSU's wave energy Linear Test Bed

Results from the simulation of the resized SeaBeavI system were used to generate 15 minute time series of the relative motion between the spar and buoy to be used as position inputs to the LTB. The sea states were selected to evaluate the performance of the linear generator over its design operating range within the limits of the LTB. Due to displacement and force limits, the maximum simulated operating condition was a 2.5 m significant wave height at a peak period of 8.8 seconds. Table 2 gives the details of the simulated time series used to drive the generator on the LTB.

Testing conditions while running the simulated time series were nearly identical to those used for the force characterization of the generator (Elwood 2008). Loading of the generator was accomplished using a three phase water rheostat and no modifications were made to the sliding surfaces. After several hours of testing, the bearing strips were worn. In some cases the stainless steel tube enclosing the magnet section was rubbing directly against the outer shell of the spar. As a result, bearing wear may have led to increased frictional forces during the testing.

Table 2: Test cases run on the LTB to determine the operating efficiency of the permanent magnet linear generator

Run	Wave Height	Period	Sea State	Resistance
non-dim	m	s	non-dim	Ohms
1	0.5	7.5	2	3.25
2	0.88	7.5	3	6
3	1.88	8.8	4	6
4	2.5	8.8	4	6

11 MODEL VALIDATION

Comparisons of the simulated time series and the measured data from the LTB have been performed in order to evaluate the accuracy of the coupled model. The error between the simulation speed and the speed generated by the test bed verified that the motor controller generated the commanded position accurately. To validate the modeling approach used to represent the generator and frictional forces in the coupled model force data from the Linear Test Bed was compared with the simulation results. The power input to the device during the LTB experiments was also compared with the mechanical power predictions from the simulation.

The data collected from the Linear Test Bed and the results of the numerical modeling were first compared graphically to evaluate the general agreement of the two data sets (see Figure 7). Error estimates for each of the quantities of interest were calculated by comparing the statistics of the simulation time series with the measured data from

the LTB. Average relative error was calculated by integrating the instantaneous error over the length of the time series:

$$AverageError = \frac{1}{T}\int_0^T \left|\frac{X_s - X_e}{X_e}\right| dt \quad (13)$$

where:

T is the length of the time series

X_s is the simulation value

X_e is the experimental value

Error analysis indicates that the motor controller on the linear test bed accurately recreated the simulated displacement on the LTB. The large force errors are likely due to a phase shift between the force measured on the test bed and the simulated force. This phase shift may be due to stiffness of the belt drive system or the load cell arms on the LTB. The error in the average power and the total energy was much lower than the force error ranging from 3.5-16.5%.

12 SYSTEM EFFICIENCY AND OPERATING LIMITS

In the resized SeaBeavI system, there are both mechanical losses due to the sliding friction between the moving components and electromagnetic losses in the generator. One of the primary goals of the coupled analysis of the system was to be able to determine the losses associated with each of the components of the system and determine which areas could be improved to benefit the system as a whole. Force and velocity data were used to determine the total mechanical power applied by the Linear Test Bed to the device. The power dissipated due to frictional losses in the bearing system was subtracted from the total power to determine the input power into the linear generator. The voltage and current measurements from the linear generator were then used to calculate the electrical power generated in order to determine the electrical efficiency.

To quantify the efficiency of the bearing system and the linear generator, the input and output power from each system was compared. The frictional force could not be measured directly so it was assumed based on the friction characteristic developed during the force characterization experimental on the LTB (Elwood 2008). Calculation of the efficiency used the following definitions for the bearing and generator efficiency:

$$Eff_{bearing} = \frac{(Power_{Mech} - Power_{Frict})}{Power_{Total}} \quad (14)$$

$$Eff_{gen} = \frac{Power_{Gen}}{(Power_{Mech} - Power_{Frict})} \quad (15)$$

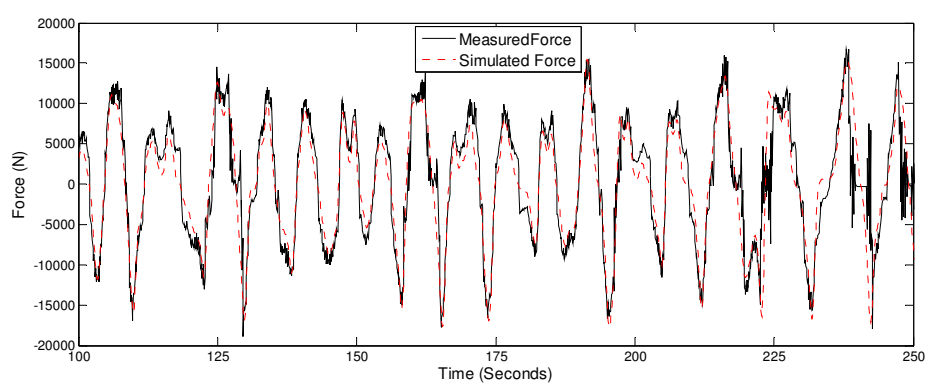

Figure 7 The sum of the frictional and electromagnetic forces in a 2.5m Hs 8.8 sec. wave climate

Table 3 Relative error between experimental measurements and OrcaFlex simulation

		Average Relative Error Between OrcaFlex and Measured Data			
Run	Hs	Position	Force	Average Power	Total Energy
non-dim	m	non-dim	non-dim	non-dim	non-dim
1	0.5	0.11%	70.57%	16.33%	16.60%
2	0.88	0.05%	46.54%	5.27%	5.41%
3	1.88	0.14%	91.94%	13.62%	13.51%
4	2.5	0.37%	136.13%	3.57%	3.68%

Table 4 Average bearing and generator efficiency as measured on the LTB

		Bearing	Generator
Run	Hs	Average Efficiency	Average Efficiency
non-dim	m	non-dim	non-dim
1	0.5	53.14%	40.94%
2	0.88	66.97%	56.37%
3	1.88	75.53%	54.70%
4	2.5	76.58%	55.03%

Efficiency of the bearing system and the linear generator were calculated using equations 17 and 18 and plotted to identify efficiency trends over the operating range. As can be seen in Figure 8, the bearing efficiency increased with increasing significant wave height. Conversely, the generator efficiency was fairly constant over the range of operating conditions investigated (Figure 9).

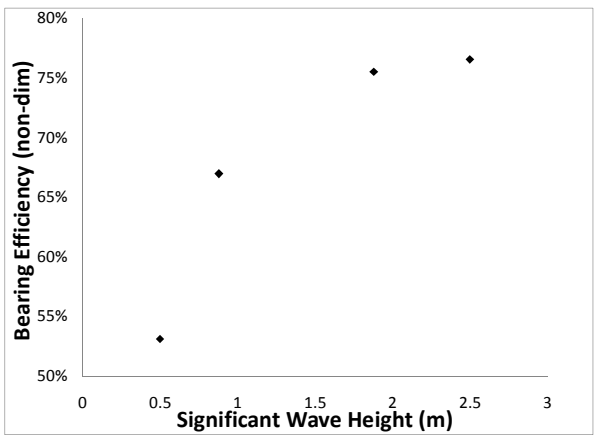

Figure 9 Measured bearing efficiency as a function of simulation wave height

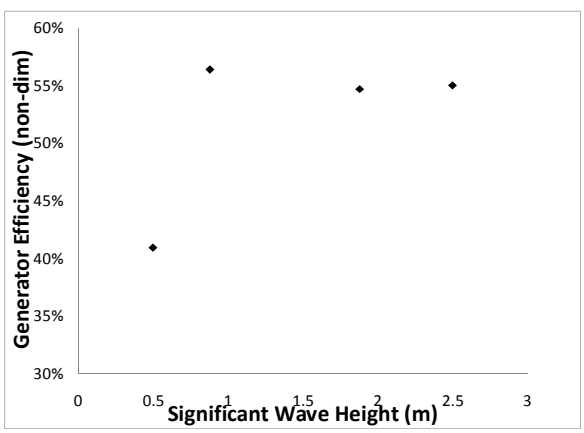

Figure 8 Measured generator efficiency as a function of simulation wave height

13 POWER CURVE AND OPERATING LIMITS

To estimate the power generation potential of the resized SeaBeavI system, a power curve was developed based on the data collected on the Linear Test Bed. A maximum operating limit was set for the device based on the limits of the tensioned mooring system. In a significant wave height greater than 4 m, the pretension in the mooring is insufficient to keep the line in tension during the down stroke of the buoy. When the significant wave height exceeds 4 m, the tension in the mooring system will be released, allowing the spar and buoy to move together over the waves. In this condition, there is still relative motion between the two floating bodies but the input power to the generator is reduced significantly. A significant wave height of .5 m was set as the lower operating limit based on the power produced during the Linear Test Bed testing.

Due to the limits of the Linear Test Bed, the bearing and generator performance was extrapolated above 2.5 m significant wave height. This extrapolated data is represented by the dotted lines in Figure 10. The bearing and generator efficiencies were assumed to remain constant from 2.5 m Hs up to the operating limit of 4.0 m Hs. This assumption is based on the efficiency curve of the linear generator which is essentially constant for significant wave heights greater than .5 m. Likewise, the efficiency curve for the bearing system reaches an asymptote for significant wave heights exceeding 2 m.

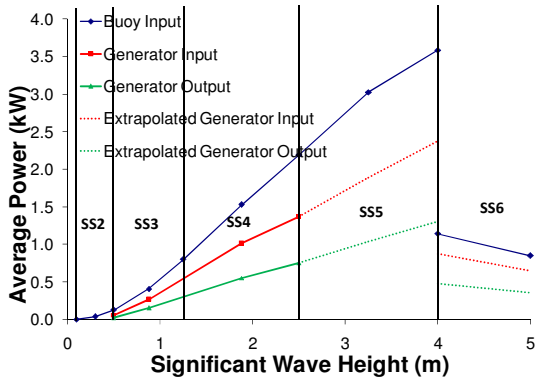

Figure 10 Power curves for the resized SeaBeavI wave energy conversion system

15 ANNUAL ENERGY PRODUCTION OFF NEPORT, OREGON

The seasonal variation in significant wave height was determined using historical data from the NDBC station over Stonewall Banks, 16 nm West of Newport, Oregon (NOAA 2008). From 1999-2004 the average daily wave height over the banks ranged

from just over 1 m in mid-August to almost 5 m in the beginning of March.

The annual energy production for the SeaBeavI operating at the OSU test site was determined using the data gathered on the wave climate off of Newport and the power curve developed for the resized device. The daily average significant wave height was used to predict the average daily energy production as seen in Figure 11.

The maximum average production predicted for the device is 32.5 kWh per day during late February. The minimum energy production occurs in mid-August when the significant wave height drops to just over 1 m. It should also be noted that there are several days in March with low energy production due to wave heights exceeding the operating limits of the device. By integrating the daily average over the course of a year the annual average energy production of the device was found to be 6322 kWh per year.

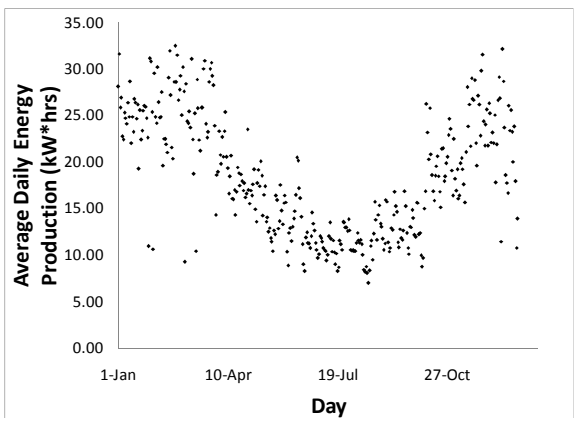

Figure 11 Resized SeaBeavI daily average energy production at Newport, Oregon test site

16 CAPACITY FACTOR

The capacity factor of a power plant is the ratio of the actual power produced over a period of time to the power it would have produced had it operated at its nameplate rating over the same period. The capacity factor for the SeaBeavI can be defined as:

$$CF = \frac{E_{actual}}{Power_{nameplate} * 365 * 24} \quad (16)$$

where:

E_{actual} is the actual annual energy produced
$Power_{nameplate}$ is the nameplate rating of the system

To calculate the capacity factor of the resized SeaBeavI, a name plate rating for the linear generator must be determined. This rating can be based either on the maximum operating condition of the wave energy system or calculated using the design current rating of the armature wires. The current rating can be used to determine the power generated at the rated current and the root mean squared velocity in the maximum operating condition. The rating of the device can be defined in this way as:

$$Power_{rnameplate} = I_{rated} V_{rated} \quad (17)$$

where:

I_{rated} is the rated current
V_{rated} is the reated voltage

Assuming a current rating of 4.68 amps and a voltage rating of 600 volts, the nameplate power of the generator is 2.81 kW. Another nameplate rating definition is the power output at the maximum operating point of the system. For the resized SeaBeavI linear generator, this maximum power output is 1.31 kW in a 4 m Hs, 9.7 Tp sea state. Using these two definitions for the nameplate rating, the capacity factor of the device is .27 and .59 respectively.

17 CONCLUSIONS AND FUTURE WORK

A coupled fluid structure interaction model of a wave energy conversion system was developed using OrcaFlex. This model was used to investigate the performance of the system over a range of operating conditions. The added mass and damping coefficients for the floating bodies were based on previous experimental and numerical results. The modeled generator loads were based on the results of force characterization experiments performed on the linear generator. OrcaFlex proved to be a capable tool for the modeling of wave energy conversion systems.

The energy production capacity of the resized SeaBeavI was determined by using simulated displacement time series from OrcaFlex to actuate the permanent magnet linear generator on the Linear Test Bed. The results of these experiments were used to develop a power curve for the device. This power curve was then used to calculate the power that could be produced given the historical wave climate off the coast of Newport, Oregon. The results of this analysis indicate that the capacity factor of the device is between .27 and .59 assuming that the device does not have to be serviced. These capacity factors are very similar to other renewable energy systems.

More work is required to refine the hydrodynamic coefficients used to model the hydrodynamics of the floating bodies in OrcaFlex. Physical experiments are required to verify the simulation results and help to refine these coefficients. A theoretical investigation of the hydrodynamics of concentric heaving bodies would enable new analytical tools to be developed that could help to optimize the configuration of the floating system. Some of this work has already been completed for concentric bodies with a large gap (Mavrakos 2004), but more work is required to extend the results to concentric bodies with small gaps.

AKNOWLEDGEMENTS

This project would not have been possible without support from the Department of Energy and our industry partner Columbia Power Technologies for their support of our research.

REFERENCES

Archimedes Wave Swing. 6 June 2008 <http://awsocean.com/>.

Budal, K. "Theory for absorption of wave power by a system of interacting bodies." Journal of Ship Research (1977): 248-253.

Chung J., G.M Hulbert. "A time integration algorithm for structural dynamics with improved numerical dissapation: The generalized-alpha method." Journal of Applied Mechanics (1993): 371-375.

Chung, J.S. "Added mass and damping of an oscillating circular column with a circular footing." International Journal of Offshore and Polar Engineering (1994): 11-17.

Curran R., L.M.C Gato. "The energy conversion performance of several types of Wells turbine designs." Proceedings of the Institute of Mechnical Engineers (1997): 133-145.

Elwood, D., E. Amon, S. Yim, A. von Jouanne, T.K.A Brekken. "Experimental Force Characterization and Numerical Modeling of a Taut-Moored Dual-Body Wave Energy Converter." Journal of Offshore Mechanics and Arctic Engineering (Submitted).

Elwood, D., J. Prudell, C. Stillinger, A. Brown, S. Yim, A. von Jouanne, T. Brekken, R. Paasch. "Design, Construction, and Ocean Testing of a Taut-Moored Dual-Body Wave Energy Converter with a Linear Generator Power Take-off." Proceedings of the 28th Annual Conferance on Offshore Mechanics and Arctic Engineering. Honolulu, Hawaii: ASME, (Submitted).

Evans, D.V. "Some theoretical aspects of three dimensional wave energy absorbers." Proceedings of the First Symposium on Wave Energy Utilization. Gothnburg, Sweden: Chalmers University of Technology, 1979. 77-106.

Falnes, J. Ocean Waves and Oscillating Systems. Cambridge, UK: Cambridge University Press, 2002.

Mavrakos, S.A. "Hydrodynamic coefficients in heave of two concentric surface-piercing truncated circular cylinders." Applied Ocean Research (2004): 84-97.

Newman, J.N. Marine Hydrodynamics. Cambridge, MA: The MIT Press, 1977.

NOAA. National Data Buoy Center. 6 June 2008 <http://www.ndbc.noaa.gov/>.

Ocean Power Technologies. Ocean Power Technologies. 6 June 2008 <http://www.oceanpowertechnologies.com/>.

Orcina Ltd. "OrcaFlex Manual." Daltongate, UK: Orcina Ltd. 2006.

Pelamis Wave Power. Pelamis Wave Power. 6 June 2008 <http://www.pelamiswave.com>.

Prudell, J.H. "Novel design and implementation of a permanant magnet linear tubular generator for wave energy conversion." Masters Thesis. Corvallis, OR: Oregon State University, 2007.

Salter S.H., D.C. Jeffery, J.R.M. Taylor. "The architecture of nodding duck wave power generators." The Naval Architect (1976).

WaveGen. WaveGen. 6 June 2008 <http://www/wavegen.co.uk>.

APPENDIX

In order to accurately model the hydrodynamic forces on the buoy and spar, values of C_{aa}, C_{an}, UDF_n, and UDF_a must be determined for each of the floating bodies. As can be seen in Figure A.1, the added mass of the buoy is constant while the damping varies with wave frequency.

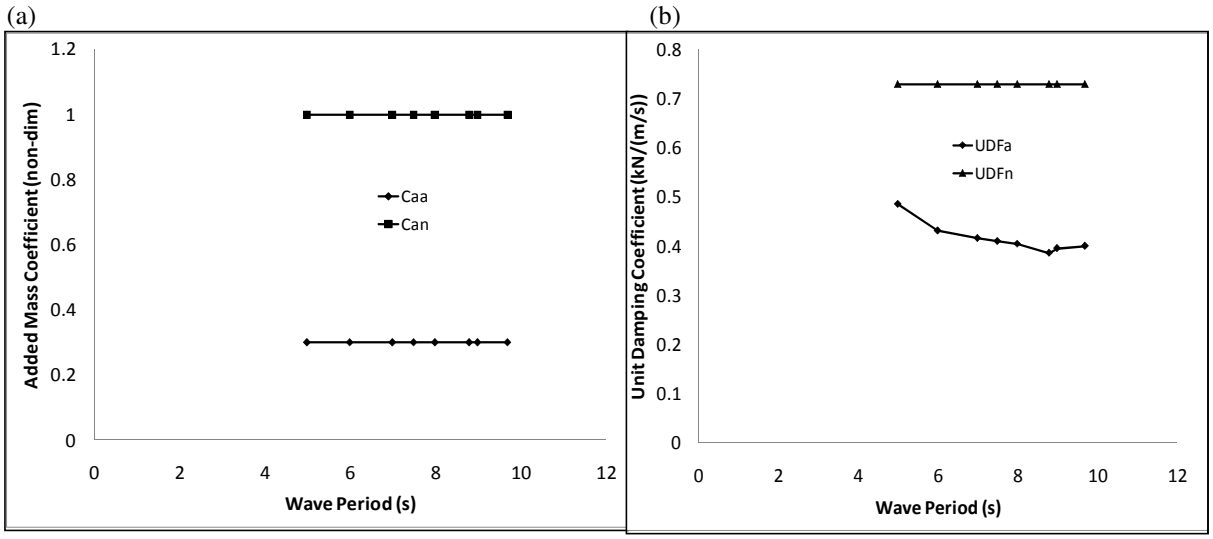

Figure A.1 (a) Axial and normal added mass coefficients for the buoy (b) Axial and normal unit damping forces for the buoy

Likewise for the spar the added mass is constant over the frequency range investigated while the heave damping is directly proportional to the wave frequency. Figure A.2 provides graphs of the added mass and damping coefficients used in OrcaFlex.

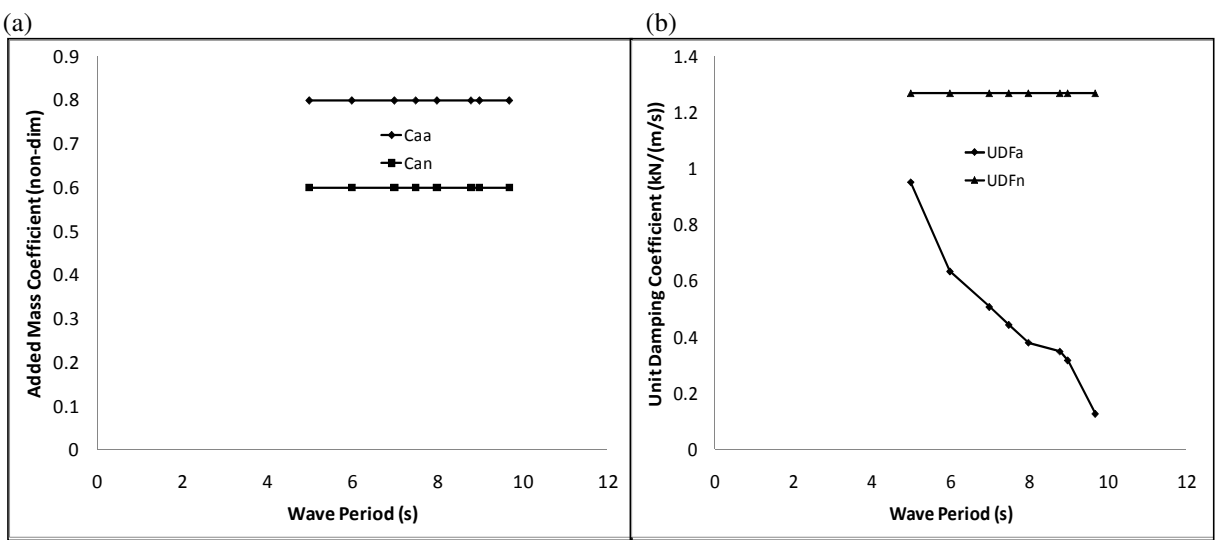

Figure A.2 (a) Axial and normal added mass coefficients for the spar (b) Axial and normal unit damping forces for the spar